16th World Congress in Computational Mechanics (WCCM)
21-26 July 2024, Vancouver, Canada
A. Korobenko, M. Laforest, S. Prudhomme, R. Vaziri (Eds)

HOW DOES FRICTION AFFECT SLIDING CONTACT MECHANICS?

NICOLA MENGA[1], GIUSEPPE CARBONE[1], CHRISTIAN MÜLLER[2], MARTIN H. MÜSER[2]

[1]Department of Mechanics, Mathematics, and Management - Polytechnic University of Bari
Via Orabona 4, Bari, 70125, Italy
nicola.menga@poliba.it and giuseppe.carbone@poliba.it

[2]Department of Materials Science and Engineering - Saarland University
Saarbrücken, 66123 Germany
chris297@gmx.de and martin.mueser@mx.uni-saarland.de

Key words: elastic coupling, friction, tribology, contact mechanics

Abstract. *Dealing with semi-infinite solids, interfacial friction is usually neglected, as normal and tangential displacements fields are independent on each other (unless material dissimilarity occurs). However, contacts involving a sufficiently thin layer, do not stick to such a simplified assumption, as thickness related normal/tangential coupling occurs, and surface frictional shear stresses do matter. It is the case, for instance, of classical rotary seals in boundary lubrication regimes, where rough frictional contacts between thin polymeric sealing lips and rotating shafts occur. Also, functional coatings to control the interface (adhesive, frictional, chemical, etc.) behavior, may be very thin and compliant, and usually experience frictional sliding during operation. All the same, these examples indicates that conditions exists where elastic coupling between in plane and out of plane displacements cannot be neglected and must be considered, instead. Here, we present our results on the rough contact mechanics of elastic and viscoelastic thin layers. We assume sliding conditions and friction at the interface, and we investigate the contact problem in the framework of linear (visco)elasticity, by relying on the Green's functions approach. We show that, due to the friction and coupling, the presence of interfacial friction may lead to a significant increase of the contact area (up to 10%), compared to the frictionless case, which may affect specific functional response of the interface, such as electrical and thermal conductivity. Since the normal gap distribution is also affected by coupling and friction, the leak rate at the interface turns out significantly altered too. Coupling and friction also affect the contact pressure, which presents a certain degree of asymmetry leading (even for purely elastic materials) to an additional interlocking contribution to the tangential force opposing the relative motion at the interface. Therefore, the overall macroscale friction cannot be predicted by summing-up the local friction contributions occurring at microscale as commonly expected; it should instead include an additional coupled-induced term. The surface stress tensor is also affected, as due to friction and coupling very high tensile stresses are localized at the contact trailing edge, which are likely to induce material failure. In conclusion, we show that the common practice to neglect in-plane interactions in contact mechanics may lead to misleading tribological predictions.*

1 INTRODUCTION

Currently, many systems across various application fields involve thin solid films. One common example is soft coatings: a thin layer of compliant material with specific characteristics is applied to a significantly stiffer substrate (considered rigid) to tailor the overall system behavior. These behaviors include chemical resistance to corrosion, changes in stiffness, damping, and frictional properties. Applications may require either low-friction coatings to reduce energy dissipation [1], or high-friction coatings to increase the grip [2].

Interest in the tribological behavior of thin solid films, often studied as compliant layers bonded to rigid bodies and indented by other rigid or deformable rough surfaces, has grown significantly in recent decades. In addition to theoretical [3-8], numerical [9-15], and experimental [16-19] studies on contact problems of semi-infinite bodies, detailed investigations have also been conducted on contacts involving thin bodies [20-24]. It is well-known that for half-space contacts, material dissimilarity induces coupling between normal and tangential displacement fields, governed by Dundurs' second constant, β, which equals $(1-2\nu)/2(1-\nu)$ if one body is rigid, where ν is the Poisson's ratio. This effect has been explored in various studies, mainly focusing on stick-slip fretting problems associated with homogeneous [25,26], layered [27], and graded [28] elastic materials, reporting significant compressibility (i.e., dissimilarity) induced in-plane and out-of-plane coupling effects on the contact stiffness.

However, studies on thin deformable layers [29-32] have shown that thickness related coupling also exists, which is not affected by the value of Dundurs' second constant β and vanishes for very thick systems (i.e., half-space). These studies, focusing on smooth single asperity contacts, have shown that interfacial friction can be a game changer in coupled conditions, eventually leading to contact pressure asymmetry. In-plane stresses and friction have also be shown to alter the adhesive peeling response of thin tapes [33,34]. Recent studies have examined rough line [35,36] and areal [37] contacts of thin layers with interfacial friction, showing that thickness dependent coupling between in-plane and out-of-plane elastic fields significantly increases the effective contact area, impacting phenomena like interfacial hydraulic impedance, electrical conductivity [38], and wear process evolution [39], as well as the overall frictional performance of the interface due to contact pressure distribution asymmetry.

In this study, we report our results [35-37] for a thin coating, sufficiently softer than the underlying rigid substrate, in frictional sliding contact (line and areal case) with a rigid profile with self-affine roughness. Our approach can be exploited both for elastic and viscoelastic coating materials, analyzing the impact of thickness related in-plane and out-of-plane coupling on overall contact behavior.

2 FORMULATION

The contact problem is illustrated in Fig. 1: it features a rigid rough profile with a fundamental wavelength λ in sliding contact with a thin elastic layer of thickness h, which is backed by a rigid substrate. Since we are interested in the long-term steady-state response of the contact, rather than dynamic or transient behaviors, we assume that the sliding speed V of the rigid indenter is much lower than the speed of sound in the elastic medium.

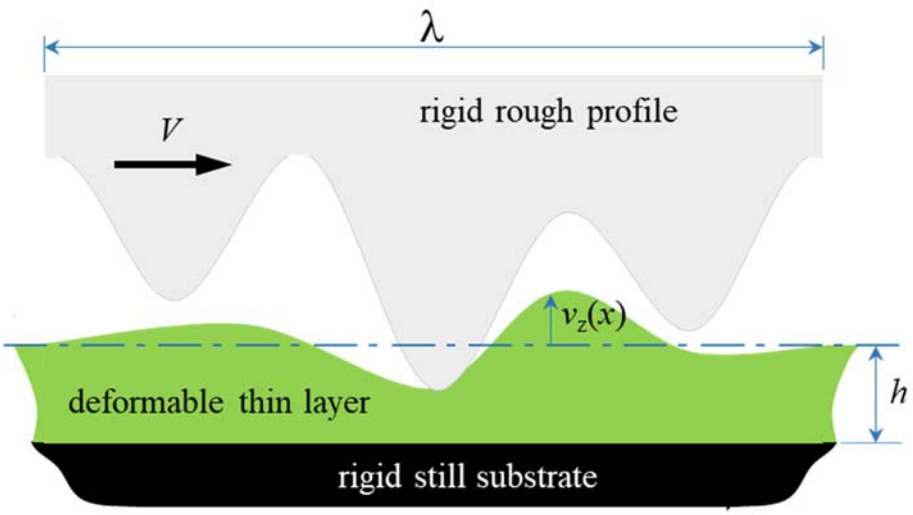

Figure 1: a rigid rough profile, of fundamental wavelength λ, in sliding at velocity V against a thin deformable layer, of thickness h, deposed onto a rigid substrate. Coulomb friction occurs at the interface, so that in-plane tractions are non-null.

Focusing on the coupled normal-tangential elastic fields in thin layers, frictional interactions at the interface are taken into account. Specifically, we use an Amonton/Coulomb friction law, allowing the calculation of the local frictional shear stress based on the local contact pressure $p(x)$ as

$$\tau(x) = \mu_c p(x) \tag{1}$$

where μ_c is the Coulomb friction coefficient, which in our formulation is assumed as independent of the sliding speed.

Focusing firstly on the line contact case, given the Green's tensor

$$\bar{\bar{\boldsymbol{G}}} = \begin{pmatrix} G_{xx} & G_{xz} \\ -G_{xz} & G_{zz} \end{pmatrix} \tag{2}$$

the contact problem can be formulated as a mixed value problem and solved by means of the procedure described in [35,36]. We have:

$$\boldsymbol{v}(x) = \frac{1}{E}\int_{\Omega} ds \bar{\bar{\boldsymbol{G}}}(x-s)\boldsymbol{\sigma}(s)\,; \qquad x \in \Omega, \tag{3}$$

where $\boldsymbol{v} = (v_x, v_z)$ is the surface displacement vector, and $\boldsymbol{\sigma} = (\tau, p)$ is the vector field of surface stress distributed over the contact domain Ω, and E is the elastic modulus (i.e., the Young's modulus).

The Green's tensor $\bar{\bar{\boldsymbol{G}}}$, as described in Eq. (2), is the key component of the present formalism. Indeed, it takes into account for the finite thickness and material compressibility of the thin deformable layer. More in details, the cross-coupled terms $G_{xz} = -G_{zx}$ are responsible of the coupling between in-plane and out-of-plane elastic fields (i.e., stresses and displacements).

In the case of line contacts, the Green's tensor terms are given as follows

$$G_{xx}(x) = -\frac{2(1-\nu^2)}{\pi}\left[log\left|2\,sin\left(\frac{q_0 x}{2}\right)\right| + \sum_{m=1}^{\infty} B(mq_0h)\frac{cos(mq_0x)}{m}\right] \tag{4}$$

$$G_{xz}(x) = \frac{1+\nu}{\pi}\left[\frac{1-2\nu}{2}[sgn(x)\pi - q_0 x] - \sum_{m=1}^{\infty} C(mq_0h)\frac{sin(mq_0x)}{m}\right] \tag{5}$$

$$G_{zz}(x) = -\frac{2(1-\nu^2)}{\pi}\left[log\left|2\,sin\left(\frac{q_0 x}{2}\right)\right| + \sum_{m=1}^{\infty} A(mq_0h)\frac{cos(mq_0x)}{m}\right] \tag{6}$$

where E is the elastic modulus (i.e., the Young's modulus), h the layer thickness, and $q_0 = 2\pi/\lambda$. Moreover, following [21,35,36], the thickness dependent series coefficients A, B, C in Eqs. (4-6) are given by

$$A(mq_0h) = 1 + \frac{2mq_0h - (3-4\nu)\,sinh(2mq_0h)}{5 + 2(mq_0h)^2 - 4\nu(3-2\nu) + (3-4\nu)\,cosh(2mq_0h)} \tag{7}$$

$$B(mq_0h) = 1 - \frac{2mq_0h + (3-4\nu)\,sinh(2mq_0h)}{5 + 2(mq_0h)^2 - 4\nu(3-2\nu) + (3-4\nu)\,cosh(2mq_0h)} \tag{8}$$

$$C(mq_0h) = \frac{4(1-\nu)[2 + (mq_0h)^2 - 6\nu + 4\nu^2]}{5 + 2(mq_0h)^2 - 4\nu(3-2\nu) + (3-4\nu)\,cosh(2mq_0h)} \tag{9}$$

The contact problem can be tackled numerically solving Eq. (3) for the unknown vector field of surface stress $\boldsymbol{\sigma}$ distributed over the contact domain Ω. This can be done enforcing the geometric condition that, due to material impenetrability, the elastic half-plane normal displacement v_x must be related to the indenter shape r within the contact domain Ω, i.e.

$$v_x(x) = \Lambda - r(x) - \Delta; \quad x \in \Omega, \tag{10}$$

where Λ is the maximum roughness height, and Δ is the contact penetration, as shown in Fig.1.

Finally, the closing condition to determine the exact contact domain Ω follows by the adhesiveless behavior of the system, which entails that the normal pressure distribution at the contact edges (i.e., the boundary $\partial\Omega$ of the contact domain Ω); therefore, $p(x) = 0$ for $x \in \partial\Omega$.

Due to the coupling between in-plane and out-of-plane elastic fields caused by the finite thickness of the deformable layer, a certain degree of asymmetry arises in the contact pressure distribution, even for purely elastic materials. This results in an additional tangential force that opposes the relative motion between the sliding rough indenter and the deformable layer, and the additional friction coefficient for this interaction can be calculated as usual for viscoelastic asymmetric contacts [13,14,22,23,36]:

$$\Delta\mu = \frac{\int_\lambda dx\, p(x) v_2'(x)}{\lambda p_m} \tag{11}$$

Notably, the same formulation can be extended to the case of a layer of viscoelastic material. Indeed, following [13,14,22,23,36], provided that the indenter sliding velocity V is constant, the contact problem can be rewritten similarly to the elastic case [i.e, Eq. (3)] as

$$\boldsymbol{v}(x) = \int_\Omega ds \bar{\bar{\boldsymbol{\Gamma}}}(x-s)\boldsymbol{\sigma}(s)\,; \quad x \in \Omega, \tag{12}$$

where the new viscoelastic Green's tensor is given by

$$\bar{\bar{\Gamma}} = \begin{pmatrix} \Gamma_{xx} & \Gamma_{xz} \\ -\Gamma_{xz} & \Gamma_{zz} \end{pmatrix} \tag{13}$$

with

$$\Gamma_{ij}(x) = J(0^+)\mathrm{G}_{ij}(x) + \int_{0^+}^{\infty} \mathrm{G}_{ij}(x + Vt)\dot{J}(t)dt \tag{14}$$

where G_{ij} (with $i,j \in \{x,z\}$) are given by Eqs. (4-6). Notably, in Eq. (14),

$$J(t) = H(t)\left[\frac{1}{E_0} - \left(\frac{1}{E_0} - \frac{1}{E_\infty}\right)e^{-t/\tau}\right] \tag{15}$$

is the material viscoelastic creep function for a single relaxation time τ, with E_0 and E_∞ being the very low-frequency (soft) and very high-frequency (glassy) elastic moduli, respectively.

3 RESULTS

3.1 Line contacts

In this section, we present our main findings on the frictional behavior of thin elastic layers in sliding contact with rough rigid profiles. Assuming Coulomb friction at the indenter-layer interface, the in-plane shear stress field is non-zero. Under these conditions, half-plane contacts would behave as in frictionless conditions (i.e, $G_{xz} = 0$); however, the finite thickness of the layer introduces a coupling between the normal and tangential elastic fields, altering both displacement fields due to interfacial friction. Specifically, in order to highlight the pure effect of the layer thickness, we set the Poisson's ratio to 0.5, therefore leading to vanishing compressibility related effects.

One significant effect of normal-tangential coupling is on the size of the real contact area between the rigid indenter and the elastic layer. In contact mechanics, it is well-known that due to surface roughness, the real contact area can be much smaller than the nominal contact area, with the ratio potentially as low as 10% for soft contact, and even below for metal contacts [11]. From early multi-asperity theories to more recent multi-scale fractal contact theories [3,4], it has been shown that the relationship between stress distribution and displacement distribution of the deformable solid is crucial in determining the real contact area's size. To this regard, normal-tangential coupling can be a game changer, as it strongly affects the mechanical behavior of thin layers interfaces compared to half-space ones.

This is clearly demonstrated in Fig. 2(a), which shows the deformed interfaces of thin elastic layers in contact with a self-affine rough profile under the same normal pressure, for both frictional (i.e., $\mu_c > 0$) and frictionless (i.e., $\mu_c = 0$) conditions. With frictional tangential stresses, the system is more compliant, resulting in a larger contact area compared to frictionless contact. Additionally, the contact penetration (i.e., the extent to which the rigid profile penetrates the deformed layer surface) is much higher with friction. Specifically, the leading edge of the contact (the right-hand contact edge in the figure) under frictional conditions is significantly shifted in the sliding direction compared to the frictionless case, while the trailing edge (the left-hand contact edge in the figure) is less affected by coupling, though a certain difference can still be reported at different values of the Coulomb friction coefficient μ_c.

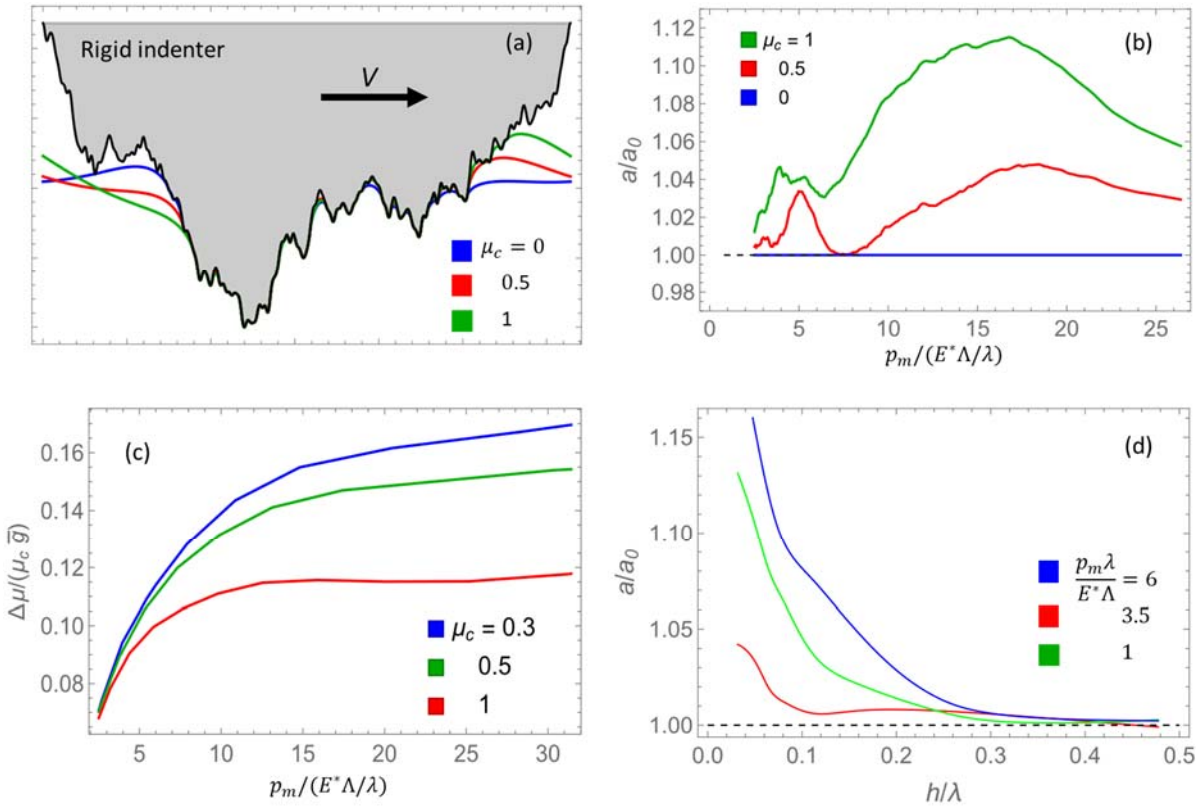

Figure 2: line contact results. (a) the effect of Coulomb friction coefficient μ_c on the normal displacements of the layer surface (results refer to $h/\lambda = 0.16$ and $p_m/(E^*\Lambda/\lambda) = 3$). (b) the normalized contact size (with a_0 being the contact size in frictionless conditions) as a function of the normalized contact mean pressure (results refer to $h/\lambda = 0.16$). (c) the normalized additional friction coefficient $\Delta\mu$ (with $\bar{g}$ being the indenter root mean square gradient) induced by coupling as a function of the normalized contact mean pressure (results refer to $h/\lambda = 0.01$). (d) the normalized contact size (a_0 refers to frictionless conditions) as a function of the normalized layer thickness (results refer to $\mu_c = 0.5$).

Quantitative conclusions can be drawn from Fig. 2 (b), which shows the ratio a/a_0 as a function of dimensionless mean contact pressure $p_m/(E^*\Lambda/\lambda)$, with a being the contact size in frictional conditions and a_0 that in frictionless sliding. The results are compared for different values of the Coulomb friction coefficient μ_c. At very low contact pressures, since only the roughness tips are involved in the contact, the statistical content of the results is reduced, which in turn leads to a certain noise in the numerics. Nonetheless, consistently with what observed in Fig. 2(a), the contact area is larger when frictional interactions occur at the contact interface, compared to the frictionless case. The increase in contact area due to friction is of engineering interest in many applications involving finite thickness bodies in sliding contact, such as tire-road interactions and the electrical conductivity of sliding electrodes. For instance, up to a 10% larger contact area can be observed with high friction coefficients typical of tire-road interfaces, and even with lower friction coefficients, the contact area increase is about 2-3%. Furthermore, Fig. 2(b) aligns with Fig. 2(a) regarding penetration differences between frictional and frictionless contacts under the same mean pressure, as a larger contact area results in a stiffer contact response due to more material being involved in deformation.

An additional friction opposing the relative sliding motion between the rigid indenter and

the elastic layer may occur due to asperities interlocking. This scenario might also involve a relative eccentricity between the pressure distribution and asperities' shape. As shown in Fig. 2, the significant asymmetry of the contact area across each asperity shifts the contact pressure distribution towards the leading edge of each contact spot. Under these conditions, interlocking friction occurs. The associated additional friction coefficient $\Delta\mu$ can be calculated using Eq. (11) and is reported in normalized form in Fig. 2(c) as a function of the dimensionless mean contact pressure $p_m/(E^*\Lambda/\lambda)$. Normalizing the interlocking friction coefficient $\Delta\mu$ by the root mean square gradient $\bar{g}$ of the rough profile is appropriate because several contact mechanics theories [3,4] suggest a proportionality between $\Delta\mu$ and $\bar{g}$. Regardless of the value of the Coulomb friction coefficient μ_c, increasing the mean contact pressure leads to higher interlocking (i.e., $\Delta\mu$ values). However, at relatively high mean pressures, $\Delta\mu$ is almost constant, as above a certain pressure, the leading edge of each contact spot can no longer shift in the sliding direction, resulting in maximum contact area eccentricity against the asperities. Additionally, given a certain surface (i.e., the value of $\bar{g}$) increasing the Coulomb friction coefficient μ_c results in a reduction of the relative additional friction coefficient $\Delta\mu/\mu_c$.

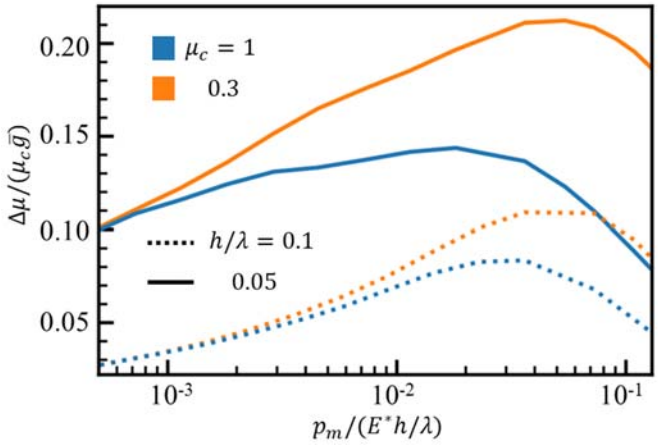

Figure 3: the normalized additional friction coefficient $\Delta\mu$ induced by coupling in areal contacts as a function of the normalized contact mean pressure ($\bar{g}$ is the indenter root mean square gradient).

Finally, Fig. 2(d) shows the effect of the normalized layer thickness h/λ on the ratio a/a_0. As predicted by Eqs. (5,8), geometrical coupling rapidly decreases with increasing layer thickness: indeed, the contact area enhancement due to in-plane and out-of-plane coupling significantly reduces with h/λ increasing. Eventually, for $h/\lambda > 0.5$, the rigid substrate is far enough from the contact interface so that weak material confinement occurs and coupling effects become negligible.

3.2 Areal contacts

Calculations have also been performed for areal contacts, exploiting GFMD contact mechanics methodology. This time, the Green's tensor is 3-dimensional and is given in Ref. [37].

Frictional results are shown in Fig. 3 where the normalized additional friction coefficient $\Delta\mu$ induced by in-plane and out-of-plane elastic coupling is reported as a function of the normalized

pressure $p_m/(E^* h/\lambda)$. Notably, we change the pressure normalization factor (with respect to Fig. 2) to simplify the results comparison against different layer thickness values, which entails different contact stiffness [20-23]. Areal contact confirm the same trend as in line contacts, with higher relative additional friction coefficient $\Delta\mu/\mu_c$ associated to lower Coulomb friction coefficient μ_c. Increasing the contact mean pressure increases the coupling-induced additional friction coefficient $\Delta\mu$ up to a peak value, while a reduction is observed at very high pressures. The main reason for this behavior is that surface gradients in Eq. (11) at the contact edges initially increase with load and, as the contact dimension grows, eventually decrease due to the sinusoidal characteristics of the roughness profile.

4 CONCLUSIONS

In this paper, we summarize our key findings on the rough contact mechanics of thin elastic layers in sliding contact with a rigid profile, for both line and areal cases. We assume local Coulomb friction at the interface, leading to coupling between the in-plane and out-of-plane elastic fields due to the finite thickness of the layer. This coupling persists even in incompressible materials, such as rubber-like polymers.

Our results indicate that the coupled behavior at the interface significantly influences both the real contact area and the overall frictional response. Specifically, we found that the contact area can increase substantially compared to the frictionless case under a given normal load. This increase is primarily due to the different displacements at the interface, allowing deeper penetration of the rigid indenter into the deformable thin layer.

Interestingly, because the displacement field and pressure distribution exhibit some eccentricity with respect to the asperities, interlocking friction occurs. This results in an additional friction term which sums to the Coulomb friction and opposes the relative sliding between the surfaces.

Acknowledgment

This work was partly supported by European Union – NextGenerationEU programs PRIN2022 grant nr. 2022SJ8HTC - ELectroactive gripper For mIcro-object maNipulation (ELFIN), and PRIN2022 PNRR grant nr. P2022MAZHX - TRibological modellIng for sustainaBle design Of induStrial friCtiOnal inteRfacEs (TRIBOSCORE). The opinions expressed are those of the authors only and should not be considered as representative of the European Union or the European Commission's official position. Neither the European Union nor the European commission can be held responsible for them.

REFERENCES

[1] Kano, M., 2006. Super low friction of DLC applied to engine cam follower lubricated with ester-containing oil. Tribol. Int. 39 (12), 1682–1685.

[2] Voigt, D., Karguth, A., Gorb, S., 2012. Shoe soles for the gripping robot: Searching for polymer-based materials maximising friction. Robot. Auton. Syst. 60 (8), 1046–1055.

[3] Persson, B.N.J., 2001. Theory of rubber friction and contact mechanics. J. Chem. Phys. 115, 3840–3861.

[4] Persson, B.N., Albohr, O., Tartaglino, U., Volokitin, A.I., Tosatti, E., 2004. On the nature of surface roughness with application to contact mechanics, sealing, rubber friction and

adhesion. J. Phys.: Condens. Matter. 17 (1), R1.
[5] Menga, N., Putignano, C., Carbone, G., Demelio, G.P., 2014. The sliding contact of a rigid wavy surface with a viscoelastic half-space. Proc. R. Soc. Lond. Ser. A Math. Phys. Eng. Sci. 470 (2169), 0392.
[6] Menga, N., Carbone, G., Dini, D., 2018c. Do uniform tangential interfacial stresses enhance adhesion? J. Mech. Phys. Solids 112, 145–156.
[7] Menga, N., Carbone, G., & Dini, D. (2019). Corrigendum to" Do uniform tangential interfacial stresses enhance adhesion?"[Journal of the Mechanics and Physics of Solids 112 (2018) 145-156]. Journal of Mechanics Physics of Solids, 133, 103744.
[8] Menga, N., Carbone, G., 2019. The surface displacements of an elastic half-space subjected to uniform tangential tractions applied on a circular area. Eur. J. Mech. A Solids 73, 137–143.
[9] Campaná, C., & Müser, M. H. (2006). Practical Green's function approach to the simulation of elastic semi-infinite solids. Physical Review B, 74(7), 075420.
[10] Medina, S., Dini, D., 2014. A numerical model for the deterministic analysis of adhesive rough contacts down to the nano-scale. Int. J. Solids Struct. 51 (14), 2620–2632.
[11] Müser, M.H., Dapp, W.B., Bugnicourt, R., Sainsot, P., Lesaffre, N., Lubrecht, T.A., Rohde, S., et al., 2017. Meeting the contact-mechanics challenge. Tribol. Lett. 65 (4), 118.
[12] Menga, N., Afferrante, L., Pugno, N.M., Carbone, G., 2018. The multiple V-shaped double peeling of elastic thin films from elastic soft substrates. J. Mech. Phys. Solids 113, 56–64.
[13] Mandriota, C., Menga, N., & Carbone, G. (2024). Adhesive contact mechanics of viscoelastic materials. International Journal of Solids and Structures, 290, 112685.
[14] Carbone, G., Mandriota, C., & Menga, N. (2022). Theory of viscoelastic adhesion and friction. Extreme Mechanics Letters, 56, 101877.
[15] Ceglie, M., Menga, N., & Carbone, G. (2024). Modelling the non-steady peeling of viscoelastic tapes. International Journal of Mechanical Sciences, 267, 108982.
[16] Homola, A.M., Israelachvili, J.N., McGuiggan, P.M., Gee, M.L., 1990. Fundamental experimental studies in tribology: The transition from ‘‘interfacial friction’’ of undamaged molecularly smooth surfaces to normal friction with wear. Wear 136 (1), 65–83.
[17] Chateauminois, A., Fretigny, C., 2008. Local friction at a sliding interface between an elastomer and a rigid spherical probe. the. Eur. Phys. J. E 27 (2), 221–227.
[18] Krick, B.A., Vail, J.R., Persson, B.N., Sawyer, W.G., 2012. Optical in situ micro tribometer for analysis of real contact area for contact mechanics, adhesion, and sliding experiments. Tribol. Lett. 45 (1), 185–194.
[19] Ben-David, O., Cohen, G., Fineberg, J., 2010. The dynamics of the onset of frictional slip. Science 330 (6001), 211–214.
[20] Putignano, C., Carbone, G., Dini, D., 2015. Mechanics of rough contacts in elastic and viscoelastic thin layers. Int. J. Solids Struct. 69, 507–517.
[21] Menga, N., Afferrante, L., Carbone, G., 2016a. Adhesive and adhesiveless contact mechanics of elastic layers on slightly wavy rigid substrates. Int. J. Solids Struct. 88, 101–109.
[22] Menga, N., Afferrante, L., Carbone, G., 2016b. Effect of thickness and boundary conditions on the behavior of viscoelastic layers in sliding contact with wavy profiles. J. Mech. Phys. Solids 95, 517–529.
[23] Menga, N., Afferrante, L., Demelio, G.P., Carbone, G., 2018a. Rough contact of sliding

viscoelastic layers: Numerical calculations and theoretical predictions. Tribol. Int. 122, 67–75.
[24] Menga, N., Putignano, C., Afferrante, L., & Carbone, G. (2019). The contact mechanics of coated elastic solids: Effect of coating thickness and stiffness. Tribology Letters, 67, 1-10.
[25] Nowell, D., Hills, D.A., Sackfield, A., 1988. Contact of dissimilar elastic cylinders under normal and tangential loading. J. Mech. Phys. Solids 36 (1), 59–75.
[26] Chen, W.W., Wang, Q.J., 2009. A numerical static friction model for spherical contacts of rough surfaces, influence of load, material, and roughness. J. Tribol. 131 (2), 021402.
[27] Wang, Z.J., Wang, W.Z., Wang, H., Zhu, D., Hu, Y.Z., 2010. Partial slip contact analysis on three-dimensional elastic layered half space. J. Tribol. 132 (2), 021403.
[28] Elloumi, R., Kallel-Kamoun, I., El-Borgi, S., 2010. A fully coupled partial slip contact problem in a graded half-plane. Mech. Mater. 42 (4), 417–428.
[29] Bentall, R.H., Johnson, K.L., 1968. An elastic strip in plane rolling contact. Int. J. Mech. Sci. 10 (8), 637–663.
[30] Nowell, D., Hills, D.A., 1988b. Tractive rolling of tyred cylinders. Int. J. Mech. Sci. 30 (12), 945–957.
[31] Jaffar, M.J., 1993. Determination of surface deformation of a bonded elastic layer indented by a rigid cylinder using the Chebyshev series method. Wear 170 (2), 291–294.
[32] Jaffar, M.J., 1997. A numerical investigation of the sinusoidal model for elastic layers in line contact. Int. J. Mech. Sci. 39 (5), 497–506.
[33] Menga, N., Dini, D., Carbone, G., 2020. Tuning the periodic V-peeling behavior of elastic tapes applied to thin compliant substrates. Int. J. Mech. Sci. 170, 105331.
[34] Ceglie, M., Menga, N., & Carbone, G. (2022). The role of interfacial friction on the peeling of thin viscoelastic tapes. Journal of the Mechanics and Physics of Solids, 159, 104706.
[35] Menga, N., 2019. Rough frictional contact of elastic thin layers: The effect of geometric coupling. Int. J. Solids Struct. 164, 212–220.
[36] Menga, N., Carbone, G., & Dini, D. (2021). Exploring the effect of geometric coupling on friction and energy dissipation in rough contacts of elastic and viscoelastic coatings. Journal of the Mechanics and Physics of Solids, 148, 104273.
[37] Müller, C., Müser, M. H., Carbone, G., & Menga, N. (2023). Significance of elastic coupling for stresses and leakage in frictional contacts. Physical Review Letters, 131(15), 156201.
[38] Zhang, X., Luo, C., Menga, N., Zhang, H., Li, Y., & Zhu, S. P. (2023). Pressure and polymer selections for solid-state batteries investigated with high-throughput simulations. Cell Reports Physical Science, 4(3).
[39] Menga, Nicola, Ciavarella, Michele, 2015. A Winkler solution for the axisymmetric Hertzian contact problem with wear and finite element method comparison. J. Strain Anal. Eng. Des. 50 (3), 156–162.